Desalination and Water Treatment
www.deswater.com
49 (2012) 404–424
November

doi: 10.1080/19443994.2012.699355
Taylor & Francis
Taylor & Francis Group

Modelling the Reverse ElectroDialysis process with seawater and concentrated brines

Michele Tedesco[a], Andrea Cipollina[a,*], Alessandro Tamburini[a], Willem van Baak[b], Giorgio Micale[a]

[a]*Dipartimento di Ingegneria Chimica, Gestionale, Informatica, Meccanica, università di Palermo, viale delle Scienze (Ed.6), 90128 Palermo, Italy*
Email: andrea.cipollina@unipa.it
[b]*FUJIFILM Manufacturing Europe BV, Oudenstaart 1, P.O. Box 90156, 5000LJ Tilburg, The Netherlands*

Received 12 March 2012; Accepted 29 May 2012

ABSTRACT

Technologies for the exploitation of renewable energies have been dramatically increasing in number, complexity and type of source adopted. Among the others, the use of saline gradient power is one of the latest emerging possibilities, related to the use of the osmotic/chemical potential energy of concentrated saline solutions. Nowadays, the fate of this renewable energy source is intrinsically linked to the development of the pressure retarded osmosis and reverse electrodialysis technologies. In the latter, the different concentrations of two saline solutions is used as a driving force for the direct production of electricity within a stack very similar to the conventional electrodialysis ones. In the present work, carried out in the EU-FP7 funded REAPower project, a multi-scale mathematical model for the Salinity Gradient Power Reverse Electrodialysis (SGP-RE) process with seawater and concentrated brines has been developed. The model is based on mass balance and constitutive equations collected from relevant scientific literature for the simulation of the process under extreme conditions of solutions concentration. A multi-scale structure allows the simulation of the single cell pair and the entire SGP-RE stack. The first can be seen as the elementary repeating unit constituted by cationic and anionic membrane and the relevant two channels where dilute and concentrate streams flow. The reverse electro-dialysis stack is constituted by a number of cell pairs, the electrode compartments and the feed streams distribution system. The model has been implemented using gPROMS®, a powerful dynamic modelling process simulator. Experimental information, collected from the FUJIFILM laboratories in Tilburg (the Netherlands), has been used to perform the tuning of model formulation and eventually to validate model predictions under different operating conditions. Finally, the model has been used to simulate different possible scenarios and perform a preliminary analysis of the influence of some process operating conditions on the final stack performance.

Keywords: Saline gradient power; Reverse electrodialysis; Modelling; Multi-scale; gPROMS

*Corresponding author.

Presented at the International Conference on Desalination for the Environment, Clean Water and Energy, European Desalination Society, 23–26 April 2012, Barcelona, Spain

1. Introduction

The increasing world energy demand during last decades, in conjunction with sustainability issues related to the large use of fossil fuels, is rapidly leading to a significant interest towards research on new possible renewable energy sources. Among the several investigated researches, a promising option is the use of salinity gradient power (SGP), also called "osmotic energy", i.e. the chemical energy potential associated with the "controlled" mixing of two salt solutions at different concentrations.

The concept of SGP is already known in the literature and was described for the first time in 1954 by Pattle [1]. Two different techniques have been proposed in the literature for recovering the osmotic energy of a system and convert it into a more exploitable form: pressure retarded osmosis (SGP-PRO) and reverse electrodialysis (SGP-RE). In the former, SGP is converted into mechanical energy (and then to electrical energy by means of turbines) using osmotic membranes, i.e. membranes allowing the passage of water and obstructing the passage of salts; in the latter, SGP is converted directly into electric energy adopting selective ion exchange membranes (IEM) within a stack similar to conventional electrodialysis ones.

In general, the overall process performance is strongly related to the concentration gradient available, e.g. river water, seawater or differently concentrated saline solutions. In particular, recently, there has been a growing interest for the use of salinity gradients generated by the mixing of seawater and very concentrated brines such as those produced in saltworks, salt mines or some other industrial activities. In this regard, it is worth mentioning the EU-FP7 funded REAPower project [2], which aims at the development of a SGP-RE unit for power production from seawater and concentrated brines.

1.1 Principle of SGP-RE

A simplified scheme of a typical SGP-RE stack is shown in Fig. 1. The key components of the system are the ion exchange membranes (IEMs), which are assembled in a stack with alternating cationic-type membrane (CEM) and anionic-type membrane (AEM). The distance between two subsequent membranes (i.e. the compartment thickness) is generally guaranteed by the use of polymeric spacers.

In particular, the repeating unit of the stack (generally called *cell pair*) consists of four elements: (i) a CEM; (ii) a compartment for the flowing concentrated solution (*concentrate compartment*); (iii) an AEM and (iv) a compartment for the flowing diluted solution (*diluate compartment*). The two solutions are forced to flow through the stack in alternate channels by means of suitably shaped inlet and outlet distribution systems. The external compartments of the stack (*electrode compartments*) contain the electrodes and the flowing electrolyte solution (*electrode rinse solution*), which also contains a suitable redox couple (e.g. Fe^{2+}/Fe^{3+} chloride).

In the scheme shown in Fig. 1, the two solutions are fed to the stack in co-current mode: in general, in membrane separation process (such as conventional electrodialysis process) it is preferable to use this configuration just to avoid significant local pressure difference between the two sides of IEMs and prevent the risk of internal leakages and mechanical stress to membranes [3].

With reference to the scheme reported in Fig. 1, the principle of SGP-RE process can be synthesised in the following: when the two salt solutions are fed to the stack, the concentration gradient between concentrate and diluate acts as driving force for the ions to diffuse across membranes. The passage of ions through a membrane is regulated by its permselectivity, i.e. the selectivity towards the passage of positively or negatively charged ions rather than others (e.g. cations pass through CEM, while anions are rejected). In ideal conditions, cations (mainly Na^+ ions in seawater solutions) flow only across CEMs, while anions (mainly Cl^- ions) pass only through AEMs, thus moving in opposite directions. These ionic fluxes across membranes constitute the ionic current through the stack, which is eventually converted into electric current at the electrodes. In fact, the role of the electrode rinse solution is to restore electroneutrality in external channels by means of redox reactions at the electrodes: in this way the electric continuity of the system is ensured and the generated electric current can be used by an external load.

1.2 State–of-the-art of modelling SGP-RE process

The earliest works regarding theoretical calculations on the SGP-RE process have been proposed by Weinstein and Leitz [4] and Forgacs and O'Brien [5]. However, these works, which also represent the first experimental demonstration of SGP-RE process technical feasibility, only presented the use of standard thermodynamics and "electrical model" equations for the estimation of theoretical obtainable power output. Moreover, results are certainly affected by the use of important simplifying assumptions relevant to solutions/membranes properties (e.g. the use of concentrations rather than activities, or neglecting the effects of concentration on physical properties).

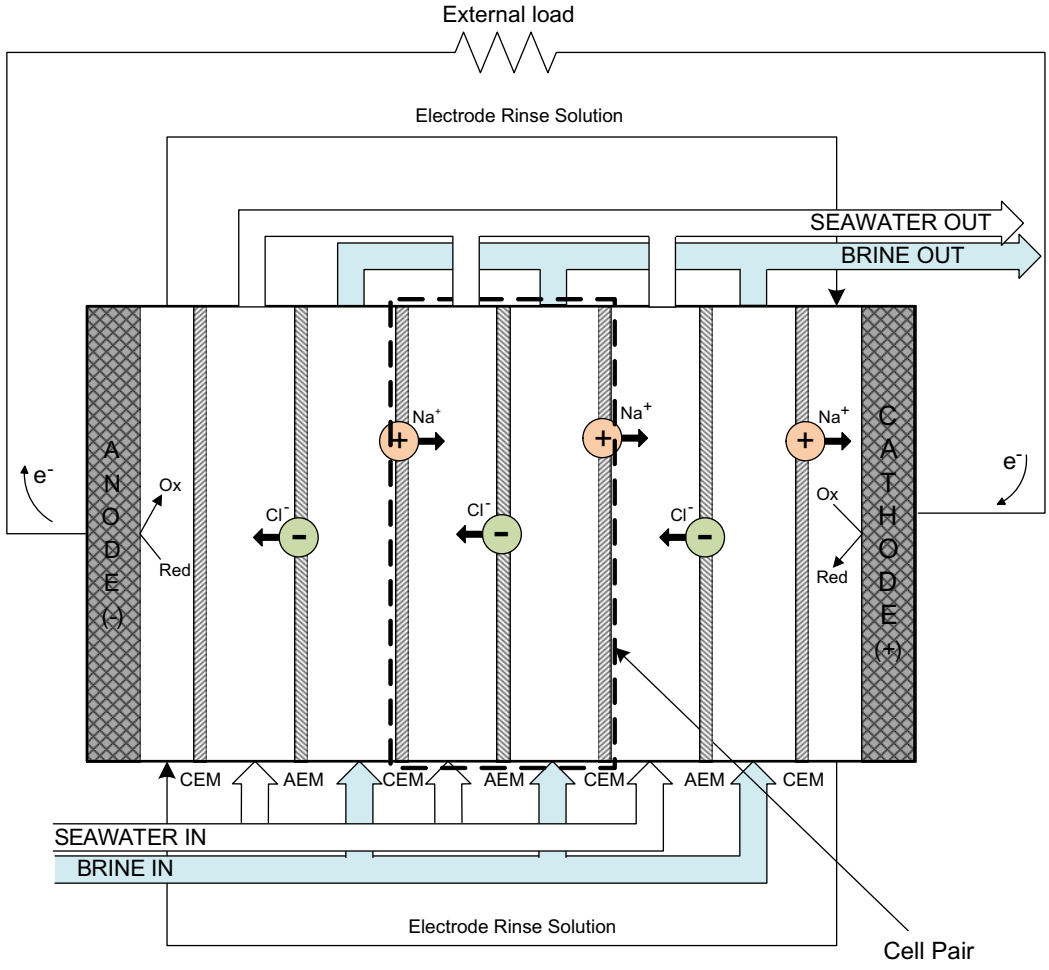

Fig. 1. Simplified scheme of a SGP-RE unit.

The first comprehensive work on SGP-RE process modelling was proposed by Lacey [6], who suggested a novel approach for estimating the cell pair voltage as the sum of electrical potential drops between the two bulk solutions through the polarisation layers, diffusive boundary layers and IEMs. This work, though lacking of any correlation for physical properties calculation, clearly demonstrated the importance of a careful equipment design for improving process efficiency. With this regard, Lacey underlined the importance of using a large concentration ratio between concentrate/dilute solutions and suitably selecting diluate concentration in order to prevent high electric resistance in dilute compartment.

Lacey's model was later modified by Brauns [7] and implemented in a solver software in order to investigate the effect of specific parameters on process efficiency. In particular, Brauns analysed the possibility of using two different thicknesses for diluate/concentrate compartments, investigating especially the effect of reducing electrical resistance by using a thinner diluate compartment. Furthermore, the effects of membrane thickness, inlet solutions concentration and temperature on cell pair voltage were investigated. Simulation results show how power output is largely affected by membrane thickness, indicating that the development of novel thinner membranes can give a significant enhancement of process efficiency.

Finally, a model for SGP-RE cell pair was proposed by Veerman et al. [8], based on thermodynamic equations for cell pair voltage calculation and transport equations coupled with electrical model equations for mass/charge flux across IEMs. The model also included three adjustable parameters, physically related to spacer shadow effects, osmotic diffusion and co-ionic flux through the membrane. A complete set of mass balance equations were also included in the model to take into account also for the variation of salt concentration along the channel due to co- and counter-ions fluxes through the membranes.

Two different "efficiency parameters" were taken into account for investigating the effect of varying operating conditions: (1) the "net power density", defined as the obtainable net power (power output minus pumping power required for pumping inlet solutions) normalised with respect to total membrane area and (2) "riverwater yield", defined as the ratio between net power and required diluate flow rate. This latter is defined assuming that the availability of river water can be a limiting factor for the process. After a suitable tuning of model adjustable parameters by comparison of purposely collected experimental information, an optimisation study was carried out with respect to these output variables, analysing the effects of compartments thickness and residence time of solutions.

On the basis of the literature review it seems clear how, although some efforts have been done already for implementing models for the SGP-RE process, these works are only related to the use of river water and seawater as feed solutions, while none of them has considered the use of concentrated brines, which could dramatically affect the model formulation. Moreover, all presented approaches are based on a number of simplifying assumptions, which could be overtaken for example by the use of a "multi-scale" approach, where different modelling scales are used to simulate different aspects of the process such as fluid flow behaviour, heterogeneity of flows distribution, transport phenomena inside cells and electrical phenomena within the entire stack.

1.3 Focus of the work

Focus of this paper is to present a multiscale model approach for the simulation of a SGP-RE stack using "seawater" and "concentrated brine" as feed solutions. In particular, an aqueous solution with a concentration of 30 g/l of NaCl (0.52 M) was considered as diluate and a 315 g/l NaCl aqueous solution (5.4 M) as concentrate stream. This last value is directly related to the real salinity of concentrated brine let out from Trapani's saltworks, where a prototype will be installed within the activities of the REAPower (*Reverse Electrodialysis Alternative Power*) EU-funded project [2].

The use of a multi-scale modelling approach is particularly suitable due to the noteworthy complexity of the process and the major goals of the modelling itself: i.e. the development of an advanced modelling tool for the optimisation of the process and the design of a SGP-RE stack to be constructed and tested within the REAPower project.

Indeed, the multiscale approach allows the mathematical description of the system at different scales, from the single cell pair to the entire stack and, eventually, to the complete plant including also auxiliary units.

Following the analysis of the state-of-the-art on SGP-RE process modelling, the cell pair model proposed in 2011 by Veerman et al. [8] for river water/seawater SGP-RE has been considered and re-adapted to the more complex case of seawater and brine. Then, starting from the cell pair model, a hierarchical structure has been implemented using gPROMS, a powerful dynamic process simulator, aiming at the modelling of the entire stack behaviour, which has been eventually validated by comparison with experimental information.

2. Model development

2.1. Development of the lower hierarchy model (cell pair)

2.1.1. System definition

A sketch of a single cell pair in co-current mode operation is shown in Fig. 2. System geometry can be characterised by four main parameters: membrane length (L) and width (b), spacer thicknesses of diluate compartment (δ_s) and concentrate compartment (δ_b).

Simplifying assumptions have been done for model implementation [8]:

(a) both solutions are assumed to be constituted only by sodium chloride (i.e. neglecting all of other ions present in real seawater/brine solutions);
(b) salt concentration profiles (in the direction perpendicular to the IEMs) are assumed to be flat in both compartments: i.e. concentration polarisation phenomena are neglected;
(c) permselectivity of both IEMs is assumed constant;
(d) *electro-osmotic flux* is considered negligible;
(e) a bi-dimensional approach has been used, thus neglecting any possible variation in the direction of channel width.

In order to take into account the non-ideality of membranes two "disturbing effects" are considered: (1) co-ions transport through the membranes and (2) solvent osmotic flux through the membranes.

The former is related to the diffusion of ions having the same charge of membrane functional groups (e.g. cations for AEMs) driven only by the concentration difference between the membrane sides. In this way, co-ions move against the main current direction,

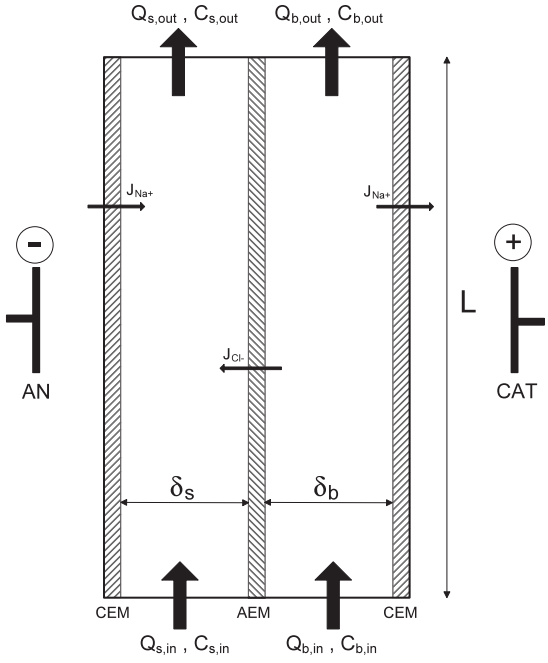

Fig. 2. Simplified scheme of a repeating unit within a SGP-RE stack (*cell pair*).

thus having a negative effect on process efficiency. On the other side, the effect of osmotic flux (from diluate to concentrate compartment) leads to a further reduction of concentration gradient between concentrate–diluate and, thus, of driving force for power production.

A "distributed parameters" model has been implemented, considering the variation of main variables (concentrations, activities, cell potentials, etc.) along the channel length (L), where a x-coordinate has been defined. Finally, all specific variables refer to the cell pair membrane area.

2.1.2. Model equations

Constitutive equations for thermodynamic properties. Veerman et al. [8] estimated activity coefficients by the Extended Debye–Hückel (EDH) equation. This well-known theory is rigorously valid only for electrolyte solutions at infinite dilution. In particular, for 1:1-valent electrolytes (such as NaCl) in aqueous solution the EDH theory gives a very good accuracy in predicting experimental trends up to a normal concentration of 0.5 eq/L [9], which is comparable with the normal concentration of seawater.

In order to estimate mean activity coefficients for electrolyte in more concentrated solutions, where concentrations range from 0.5 eq/L up to values close to saturation, a virial equation proposed by Pitzer [10] has been used:

$$\ln \gamma_{\pm} = f^{\gamma} + mB^{\gamma} + m^2 C^{\gamma} \tag{1}$$

where $\gamma_{\pm}$ and m are the mean activity coefficient and molality of the electrolyte, respectively. The term (f^{γ}), taking into account long-range forces between ions, is directly derived from EDH theory; while the second and third virial coefficients (B^{γ}, C^{γ}) are related to short-range interactions. For the estimation of these two binary interactions parameters (α, b) are adopted, which depend on the nature of the electrolyte and can be easily found in the open literature for the most common substances. For the sake of brevity, relevant expressions are not reported, but can be easily found the literature [10]. To confirm what is stated above, Fig. 3 shows a comparison between predicted and experimental values of mean activity coefficient for NaCl as a function of electrolyte concentration. It is worth noting how, for molar concentration above 0.5 M, EDH theory, predicting a monotone trend for $\gamma_{\pm}$, is not able to give accurate values of activity coefficient, while a good agreement with experimental trend is observed for the Pitzer equation.

Another physical property to be estimated for modelling purposes is the equivalent conductivity. It can significantly vary with concentration, especially when it is far from the infinite dilution condition. For this reason, while in Ref. [8] equivalent conductivity was assumed constant, in the present work concentration influence on conductivity has been considered.

Among the various correlations proposed in literature, the most accurate for NaCl solutions is the one suggested by Islam et al. [12,13], which is based on the Debye–Hückel–Onsager theory:

$$\Lambda = \left[\Lambda^0 - \frac{B_2'(c)\sqrt{c}}{1 + B'(c)a\sqrt{c}}\right]\left[1 - \frac{B_1'(c)\sqrt{c}}{1 + B'(c)a\sqrt{c}}F'(c)\right] \tag{2}$$

where Λ^0 is the equivalent conductivity at infinite dilution and c is electrolyte molar concentration; the other terms of Eq. (2) (whose definitions are not reported herein for the sake of brevity) are functions of concentration as well as some physical properties of solution itself, such as viscosity (η) and dielectric constant (ε). Thus, in order to evaluate Λ reliable data for η and ε at different salt concentrations are needed: e.g. for a 5 M NaCl solution ε is roughly 50% lower than for pure water [9]. In this paper, the effect of electrolyte concentration on η and ε has been considered assuming a linear trend with salt concentration for both [11].

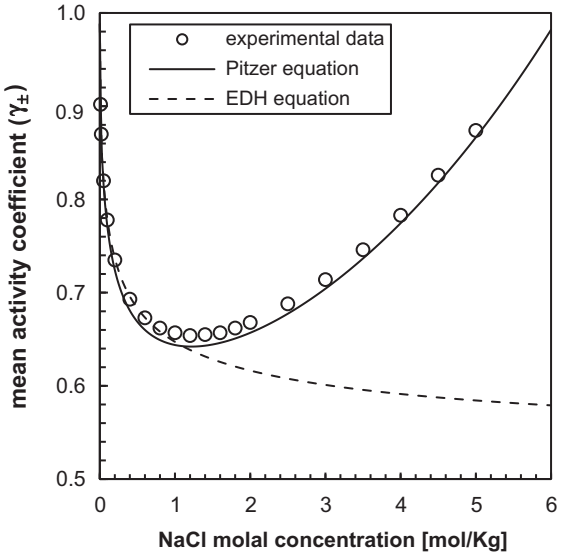

Fig. 3. Influence of NaCl molal concentration on mean activity coefficient.
Comparison between values predicted by EDH, Pitzer equation and experimental data. Experimental data from Ref. [11].

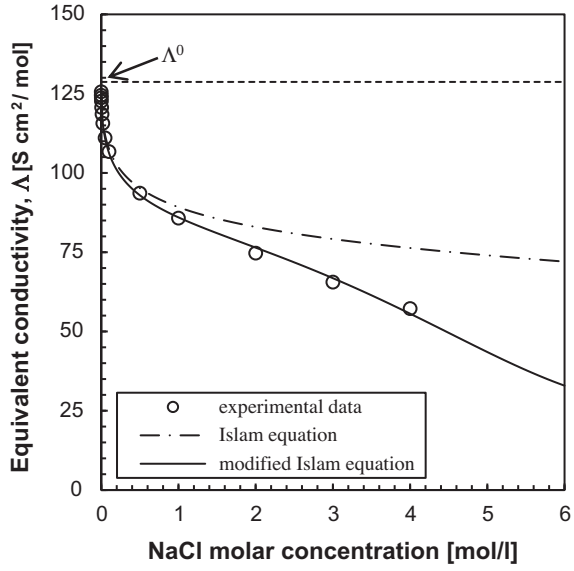

Fig. 4. Equivalent conductivity of NaCl aqueous solution. Comparison between values predicted by Islam equation, modified Islam equation and experimental data. Experimental data from Ref. [11].

Fig. 4 shows the estimated equivalent conductivity for NaCl solution at different molar concentration; note that, assuming a constant value for both η and ε, the accordance with experimental data is acceptable only for concentration lower than 1 M, while a very good matching can be achieved with the assumed linear dependence of these parameters with the concentration.

Electric variables. The open circuit voltage (OCV) of the system, i.e. the potential difference created at both IEMs, can be calculated by an equation formally similar to the Nernst equation [8]:

$$E_{\text{cell}}(x) = \alpha_{\text{CEM}} \frac{RT}{F} \ln \frac{\gamma_{\text{b}}^{\text{Na}}(x) C_{\text{b}}(x)}{\gamma_{\text{s}}^{\text{Na}}(x) C_{\text{s}}(x)} + \alpha_{\text{AEM}} \frac{RT}{F} \times \ln \frac{\gamma_{\text{b}}^{\text{Cl}}(x) C_{\text{b}}(x)}{\gamma_{\text{s}}^{Cl}(x) C_{\text{s}}(x)} \quad (3)$$

where α_{AEM}, α_{CEM} are the permselectivity of both IEMs, and the subscripts b and s are referred to brine and seawater, respectively.

The total cell pair resistance is constituted by the sum of 4 resistances in series:

$$R_{\text{cell}}(x) = R_{\text{b}}(x) + R_{\text{s}}(x) + R_{\text{CEM}} + R_{\text{AEM}} \quad (4)$$

where R_{b} and R_{s} are electrical resistances of solutions, while R_{CEM} and R_{AEM} are the IEMs resistances; in Eq. (4) all terms are expressed as areal resistances ($\Omega\,\text{m}^2$), as normally done for this kind of systems. As it concerns solutions resistances, they are calculated by:

$$R_{\text{b}} = f \frac{\delta_{\text{b}}}{\Lambda_{\text{b}} C_{\text{b}}(x)} \quad (5)$$

$$R_{\text{s}} = f \frac{\delta_{\text{s}}}{\Lambda_{\text{s}} C_{\text{s}}(x)} \quad (6)$$

where f is called *obstruction factor* and represents a correction term which takes into account the increase of electrical resistance caused by the presence of the spacer (e.g. due to tortuosity of ion path or shadow effect on membranes).

Transport equations across IEMs. The concentration gradient across each membrane generates the transport of ions from concentrate to dilute compartment. In general, because of the non-ideality of membranes, both counter-ions and co-ions will pass through each IEM; as a consequence, the total salt flux across IEMs can be divided in two terms (Eq. (7)):

$$J_{\text{tot}}(x) = J_{\text{coul}}(x) + J_{\text{cit}}(x) \quad (7)$$

in Eq. (7) the first term (counter-ions or "coulombic" flux, J_{coul}) represents the ions flux responsible of the

electric current in external circuit: this contribution can be related to the current density (j) simply by the Faraday's law. The second term, related to co-ions transport (J_{cit}), only represents a loss of driving force for SGP-RE process and herein is described through a phenomenological expression. Thus Eq. (7) can be further developed as:

$$J_{tot}(x) = J_{coul}(x) + J_{cit}(x) = \frac{j(x)}{F} + 2\frac{D_{NaCl}}{\delta_m}[C_b(x) - C_s(x)] \quad (8)$$

where j is the current density, δ_m is membrane thickness (assumed equal for both IEMs) and D_{NaCl} is the co-ions diffusion coefficient; the factor 2 allows to take into account both IEMs of a cell pair.

In Eq. (8) the D_{NaCl} term, formally analogous to a salt diffusion coefficient, could be considered strictly as the mean value of co-ions diffusivities in each membrane (i.e. Na^+ diffusivity in AEMs and Cl^- diffusivity in CEMs, respectively). While, in Ref. [8] D_{NaCl} was considered and adjustable parameter, in the present model formulation, it has been estimated from permselectivity definition itself. In fact, the definition of CEM permselectivity commonly accepted in literature [3] is:

$$\alpha_{CEM} = \frac{T_c^{CEM} - T_c}{T_a} \quad (9)$$

where T_c^{CEM} is the transport number of cation into the membrane, while T_c and T_a are cation and anion transport number in solution, respectively. Assuming only Na^+ and Cl^- ions, T_c^{CEM} should be equal to the ratio between the counter-ion molar flux (J_{coul}) and the total salt flux (J_{tot}):

$$T_c^{CEM} = \frac{z_c J_c}{\sum_i z_i J_i} = \frac{J_{coul}}{J_{coul} + J_{cit}} \quad (10)$$

substituting Eqs. (8) and (10) in Eq. (9) and rearranging, D_{NaCl} can be finally expressed as:

$$D_{NaCl}(x) = \frac{1}{2}\left[\frac{1 - T_c^{CEM}}{T_c^{CEM}}\right]\frac{j(x)}{F}\frac{\delta_m}{(C_b(x) - C_s(x))} \quad (11)$$

note that, in case of ideal membrane, $T_c^{CEM} = 1$ and therefore co-ions diffusion coefficient is zero.

Osmotic transport. Osmotic transport of solvent can be considered as proportional to the salt concentration gradient between concentrate–dilute compartment through a phenomenological expression (Eq. (12)):

$$J'_w(x) = -2\frac{D_w}{\delta_m}[C_b(x) - C_S(x)] \cdot \left(\frac{M_{H_2O}}{\rho_{H_2O}}\right) \quad (12)$$

where D_w is the water diffusion coefficient through IEMs, M_{H_2O} and ρ_{H_2O} are solvent molar weight and density, respectively, and the multiplying factor (M_{H_2O}/ρ_{H_2O}) is added in order to express J'_w as a volumetric flux ($m^3/m^2\,s$).

Mass balance. Mass balance equations for NaCl in each compartment can be easily expressed as:

$$\frac{dC_s(x)}{dx} = \frac{b}{Q_s}J_{tot}(x) \quad (13)$$

$$\frac{dC_b(x)}{dx} = -\frac{b}{Q_b}J_{tot}(x) \quad (14)$$

where Q_s, Q_b are the solution flow rates in single channel. In order to include also the effect of solvent osmotic transport mass balance can be modified, as already reported in Ref. [8]:

$$\frac{dC_s(x)}{dx} = \frac{b}{Q_s}J_{tot}(x) - C_s(x)\frac{b}{Q_s}J'_w(x) \quad (15)$$

$$\frac{dC_b(x)}{dx} = -\frac{b}{Q_b}J_{tot}(x) + C_b(x)\frac{b}{Q_b}J'_w(x) \quad (16)$$

indicating a further reduction of concentration in the concentrate compartment and an increase in the diluate one, as physically expected.

2.2. Definition of the adjustable parameter

In the model proposed by Veerman et al. [8], the obstruction factor (f) and diffusion coefficients of water and salt (D_w, D_{Nacl}) were used as adjustable parameters. In particular, f appears within calculation of areal resistances of solutions (Eqs. (5) and (6)). The influence of f on overall process efficiency, together with its possible use as adjustable parameter for the model, could be an important point to discuss. In fact when river water is used as dilute, the areal resistance of dilute solution is

the controlling resistance for the system, as already underlined by several authors [7,14]; thus it is clear that the obstruction factor has a great influence on fitting in that case.

On the other hand, concerning the conditions investigated in this work (SGP-RE process with seawater–brine) the higher salt concentration within the channels makes the areal resistance of both solutions (R_s, R_b) negligible with respect to IEMs resistances (R_{CEM}, R_{AEM}). Therefore, the effect of the obstruction factor on the overall process efficiency becomes poor and its value has been set as done by Veerman et al. (i.e. $f = 2.5$), after assessing its negligible influence on the process performance. For similar reasons, also D_w has been fixed to the literature value (i.e. $D_w = 1 \times 10^{-9}\,m^2/s$) [8]. While D_{NaCl} has been eliminated by as indicated above (Eq. (11)).

A new adjustable parameter (more suitable to the fitting) has been added to the model, in order to correct nominal values of permselectivities of IEMs to take into account of the effects of high solution concentrations, thus estimating a "corrected" OCV from Eq. (3):

$$E_{cell}(x) = \beta \cdot (\alpha_{CEM} + \alpha_{AEM}) \frac{RT}{F} \ln \frac{\gamma_b(x) C_b(x)}{\gamma_s(x) C_s(x)} \tag{17}$$

where β is the permselectivity correction factor. Note that in this simplified case (one single electrolyte in solution), the two terms on second member in Eq. (3) can be lumped together. Notwithstanding its definition, β can be seen also as a fitting parameter for taking into account any non-ideal effect related to the membranes, e.g. the shadow effect generated by the spacer filaments in contact with the membrane surface.

2.3. Development of the higher hierarchy model (stack)

Once the model for cell pair has been developed, the next step is the construction of a model for the entire stack, i.e. a system constituted by a generic number N of cell pairs plus the electrode compartments. While transport phenomena through IEMs are considered within each cell pair model, the main variables within the "stack model" are the electric variables that can be estimated only after a complete mathematical description of the entire system.

The total stack resistance is the sum of cells resistances plus the resistance in electrode compartments (*blank resistance*, R_{blank}):

$$R_{stack}(x) = \left(\sum_{i=1}^{N} R_{cell,i}(x) \right) + R_{blank} \tag{18}$$

of course, the contribution of electrode compartments on total stack resistance is relevant only for stack with small number of cells (e.g. in lab-scale units).

The potential difference available at the stack will be the sum of the OCV in all cells minus the potential drop due to the internal stack resistance:

$$E_{stack}(x) = \left(\sum_{i=1}^{N} E_{cell,i}(x) \right) - R_{stack}(x) \cdot j(x) \tag{19}$$

Then, the current density can be calculated by Ohm's law:

$$j(x) = \frac{E_{stack}(x)}{R_u} \tag{20}$$

where R_u is the external load of the system (assumed as constant), expressed in $\Omega\,m^2$.

Aside from the OCV, another useful quantity just to express the efficiency of a SGP-RE system is represented by the specific power, or power density, which is defined as the obtainable electric power per membrane area of cell pair. This variable represents the available output power normalised with respect to the required membrane surface (which is one of the principal cost issue for the process itself) and can be calculated as:

$$P_d(x) = \frac{1}{N} j^2(x) \cdot R_u \tag{21}$$

note that in Eq. (21) power density is defined with respect to the cell pair area.

The output electrical power obtainable from the stack (P_{out}), is then calculated by Joule's law as product of average stack voltage and average electric current ($P_{out} = \bar{E}_{stack} \cdot \bar{I}$) or by multiplying P_d by the total stack cell pair area.

The total required power for pumping the feed solutions through the stack can be estimated as:

$$P_{pump} = \frac{\Delta P_b \cdot Q_b^{tot} + \Delta P_s \cdot Q_s^{tot}}{\eta_p} \tag{22}$$

where ΔP is the total pressure drop (Pa), Q^{tot} is the solution flowrate (m^3/s), η_p is the pump efficiency, subscripts b and s refer to brine and seawater, respectively.

Hence, the net power, which is the obtainable electric power subtracting the required pumping power, can be estimated as:

$$P_{net} = P_{out} - P_{pump} = (\bar{E}_{stack} \cdot \bar{I}) - \frac{\Delta P_b \cdot Q_b^{tot} + \Delta P_s \cdot Q_s^{tot}}{\eta_p} \quad (23)$$

2.4. Model implementation and simulating approach

The proposed DAEs set has been implemented in gPROMS®, a powerful software for simulation (both in steady state and dynamic conditions) and optimisation of complex processes [15]. Furthermore, unlike common flow-sheeting software, which is used to carry out simulations of chemical processes with standard equipments, gPROMS allows custom mathematical description of new systems by writing model equations within the simulation software itself. Once the new equipment model has been implemented, it can be eventually connected with other units (e.g. pumps, measuring instruments, etc.), performing simulation of the entire plant.

Several useful tools are also contained in gPROMS to help the user during model building: in particular, all information describing the system (variables, parameters and equations) must be declared in different entities following a hierarchical sequence (as shown in Fig. 5). In this way, a highly structured model is built, which allows the analysis of system behaviour under different conditions.

In the present case, the model has been implemented in two hierarchical levels (*cell pair* and *stack*). Input data used in simulation are summarised in Table 1.

Finally, the *x*-domain has been discretised in 50 elements, each one with a length dx = 2 mm, thus providing information on variables along the whole compartments.

3. Experimental

3.1. Experimental set-up and procedure

In order to validate the proposed model, experimental measurements of voltage and power density were carried out on a lab-scale stack, at FUJIFILM laboratories in Tilburg (the Netherlands), using different type of commercial spacers. A simplified scheme of the experimental apparatus is shown in Fig. 6. The adopted equipment has a standard design for electrodialysis process (Deukum GmbH, Germany), with

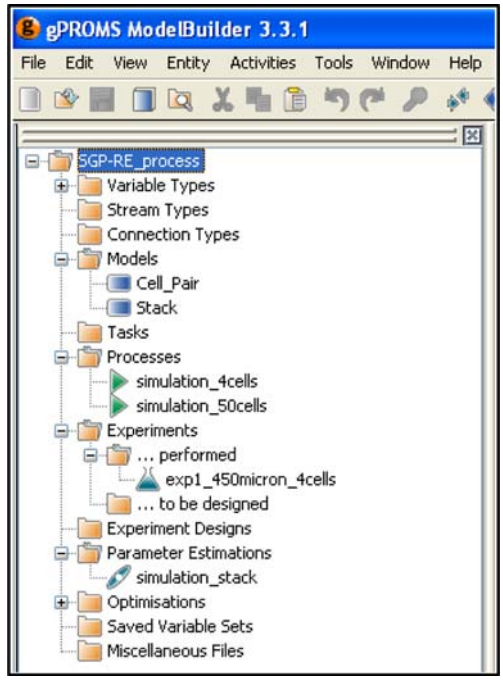

Fig. 5. Model structure within gPROMS® Model Builder.

electrodes of DSA-type. Membranes are FUJIFILM manufactured ion-exchange membranes with 10 cm × 10 cm nominal dimensions (open area); other relevant physical properties of IEMs are listed in Table 2. Woven spacers with two different nominal thickness (365 and 450 μm) were used in order to investigate the effect of channel thickness on process efficiency and to validate the model at different conditions. Two peristaltic pumps (Hosepump Masterflex PW, Burt

Table 1
Summary of input data implemented in gPROMS

Input variables
Seawater inlet concentrations
Brine inlet concentrations
Seawater feed flow rate
Brine feed flow rate
Parameters
Membrane properties
CEM permselectivity
AEM permselectivity
CEM areal resistance
AEM areal resistance
CEM/AEM thickness
Cell geometry
Cell pair length and width
Seawater/brine compartments thickness

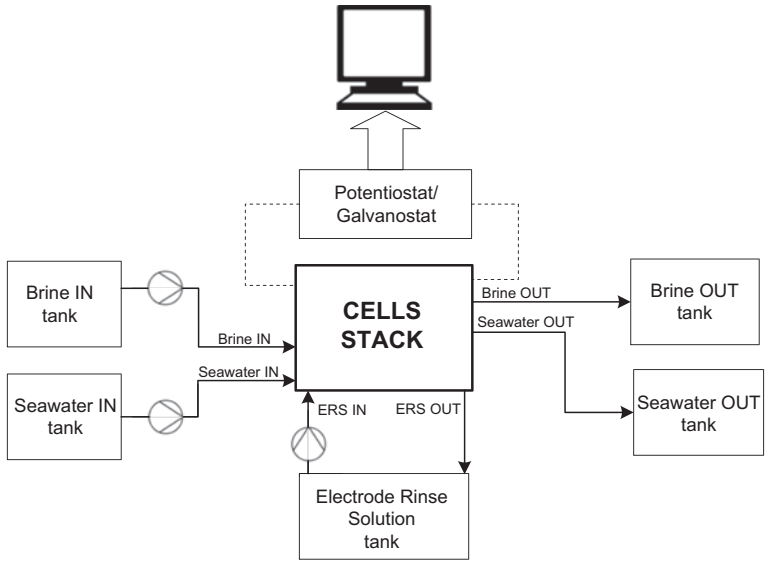

Fig. 6. Scheme of experimental set-up.

Table 2
Physical properties of used membranes

Membrane	Permselectivity[a] (%)	Areal resistance ($\Omega\,cm^2$)	Thickness (μm)
CEM	90	2.6	120
AEM	65	1.1	120

[a]Values measured with NaCl solutions 0.5 M for diluate and 4 M for concentrate.

Process Equipment Inc., USA) were used to allow circulation of both solutions through the stack; an additional pump of the same type was used for circulation of electrode rinse solution.

Measurements were carried out using 0.5 M NaCl aqueous solution as "artificial seawater" and 5.4 M NaCl aqueous solution as "artificial brine". An aqueous solution of $K_3Fe(CN)_6/K_4Fe(CN)_6$ 0.1 M and NaCl 2.5 M was used as electrode rinse solution: the addition of NaCl (with a concentration between 0.5 and 5.4 M) allowed the reduction of concentration gradient between electrode/central compartments, as well as the improvement of conductivity of the electrode rinse solution itself.

The stack was connected to feed hydraulic circuits by manifolds and to the measuring instrument (Autolab potentiostat/galvanostat PGSTAT100, Metrohm, USA) through electrical terminals connected with electrodes. A picture of experimental set-up is shown in Fig. 7, in which it is possible to see the cells stack, as well as the other relevant elements of the system.

Experimental measurements consisted of standard cyclic voltammetric analyses in galvanostatic mode [16]: in particular, each measurement was carried out imposing a ramp for the current from 0 to −0.2 A with a step of −0.5 mA/s; the measuring instrument records the potential difference (stack voltage) at terminals (Fig. 8). Each proof was repeated three times in order to guarantee reproducibility of the measurement. Once the stack voltage is measured, the stack

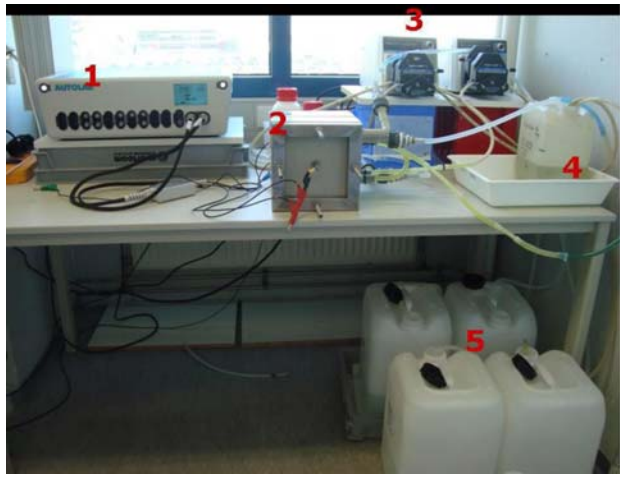

Fig. 7. Experimental set-up.
(1) Potentiostat/galvanostat; (2) cells stack; (3) pumps; (4) electrode rinse solution tank and (5) seawater/brine inlet–outlet tanks.

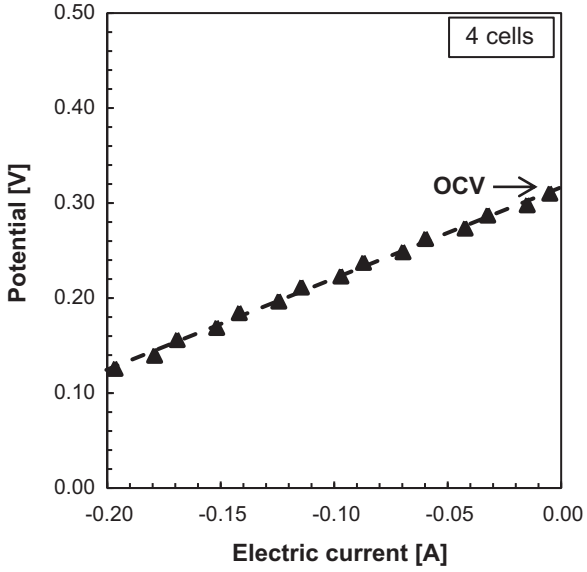

Fig. 8. Ciclic voltammetry galvanostatic on a stack equipped with four cells.
Stack equipped with 450 μm spacers in electrode/central compartments; flow rate in single channel: 13 mL/min.

resistance can be easily calculated regarding Ohm's law (Eq. (19)). In fact, R_{stack} represents the slope of the experimental curve in the graph E_{stack}/I presented in Fig. 8, while the intercept with the y-axis represents OCV for the system. Finally, electric power was

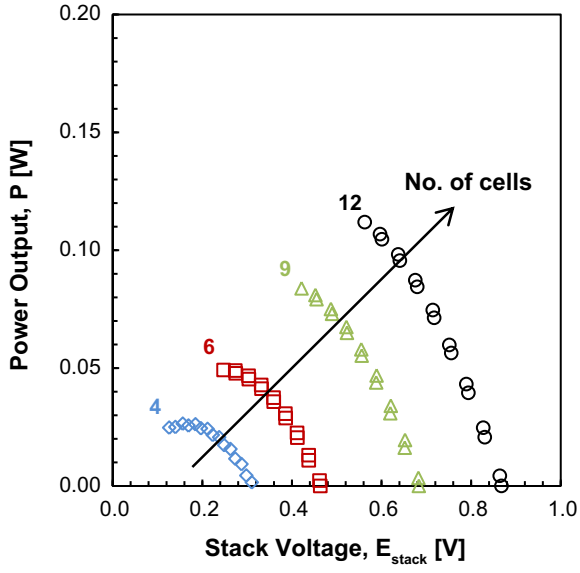

Fig. 10. Electric power for SGP-RE stack at different number of cells.
Exp measurements with 4-/6-/9-/12-cells stack equipped with 450 μm spacers in electrode/central compartments; flow rate in single channel: 13 mL/min.

calculated as the product of stack voltage and applied current, and power density was estimated normalising the latter with respect to membrane area and cells number.

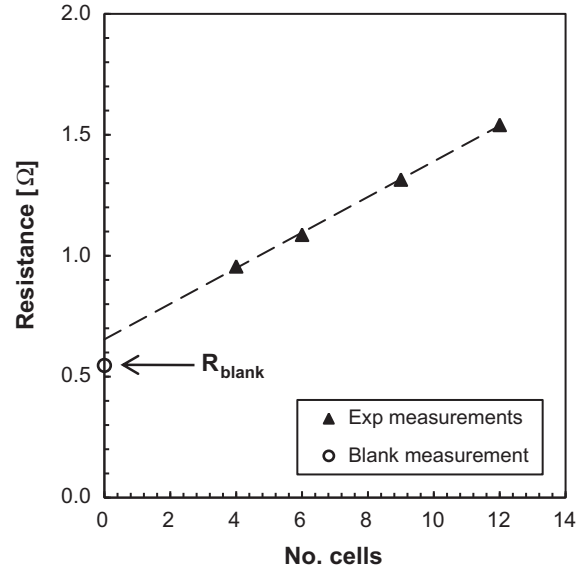

Fig. 9. Experimental measurements of stack and blank resistance.
Exp measurements with 4-/6-/9-/12-cells stack equipped with 450 μm spacers in electrode/central compartments; flow rate in single channel: 13 mL/min. Blank measurement is related to a stack equipped only with 1 CEM and 2 end-spacers.

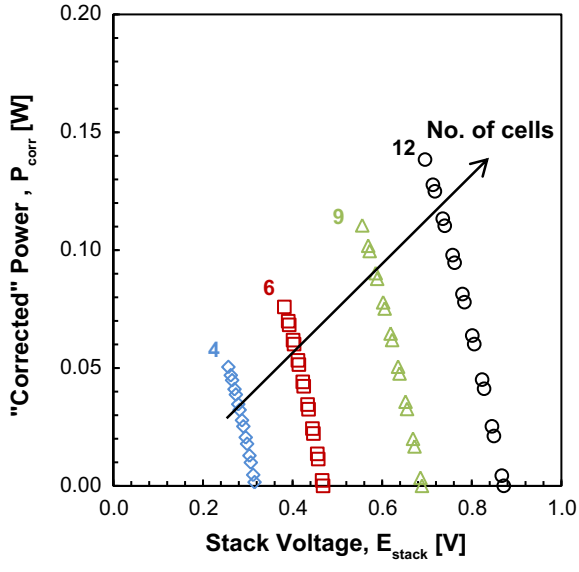

Fig. 11. "Corrected" power for SGP-RE stack at different number of cells.
Exp measurements with 4-/6-/9-/12-cells stack equipped with 450 μm spacers in electrode/central compartments; flow rate in single channel: 13 mL/min.

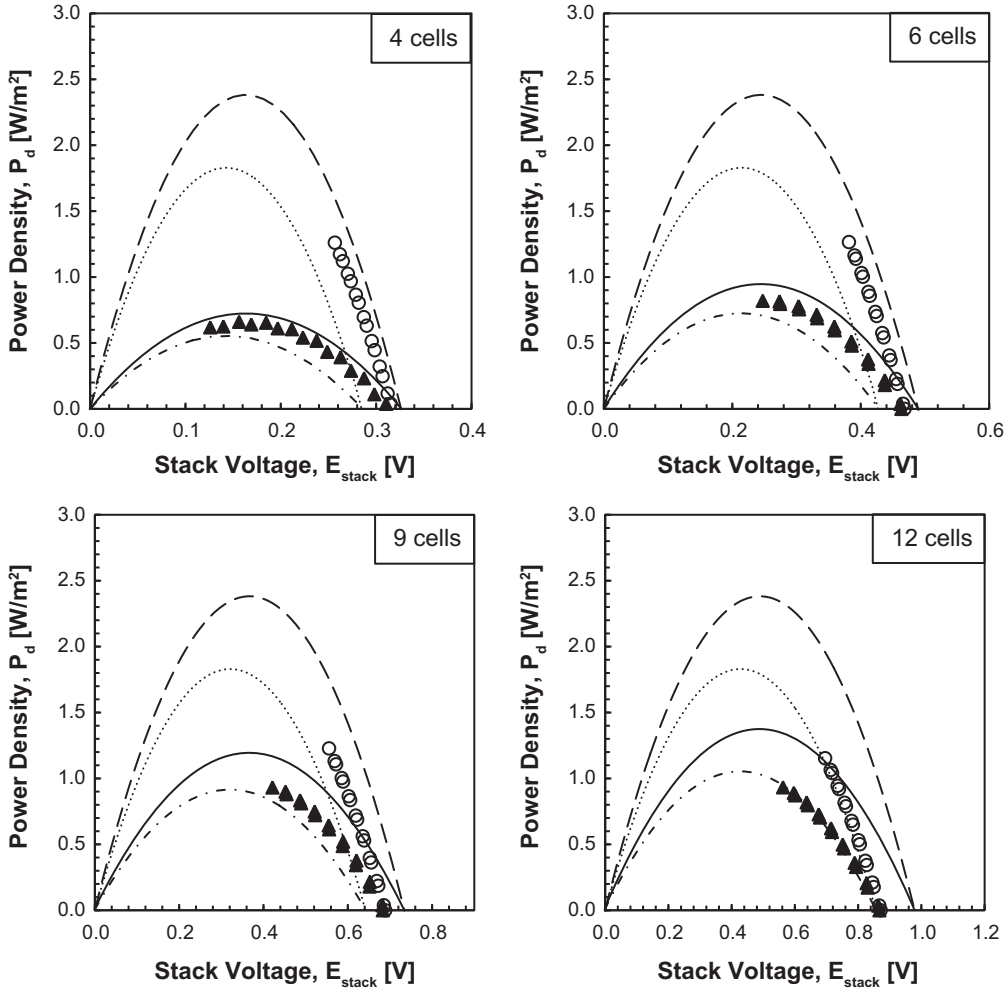

Fig. 12. Model validation for cells stack equipped with 450 μm spacers at different number of cell pairs.
▲ Experimental data; ○ "Corrected" data; Model predictions: –·–·– $\beta = 0.7$; ____ $\beta = 0.8$; Model predictions for 200 cells stack: ..... $\beta = 0.7$; _ _ _ $\beta = 0.8$.

3.2. Experimental measurements

3.2.1. Electrode compartments (blank) resistance

Experimental measurements of stack voltage are clearly affected also by the resistance of electrode compartment (R_{blank}). In order to be able to correct the measurements for obtaining the generic cell pair voltage (i.e. the voltage theoretically obtainable with a negligible blank resistance), R_{blank} must be estimated. Evaluation of blank resistance was performed from the experimental measurements of stack resistance with different number of cell pairs (Fig. 9). In fact, as indicated by Eq. (18), R_{blank} can be considered as the resistance of a "0-cells" stack and therefore can be evaluated by extrapolation of experimental data in a graph R_{stack}/N.

Measurements were carried out using stacks equipped with 450 μm spacers and with 4–6–9–12 cell pairs. Feed solutions flow rate was regulated in order to maintain a constant flow rate in single channel between 11 and 13 mL/min (corresponding to a linear velocity close to 1 cm/s). Results are shown in Fig. 9.

Blank resistance was also directly measured carrying out a cyclic voltammetry on a stack equipped only with the two end-spacers and a single CEM between them. The latter is added to avoid the passage of electrode rinse solution directly from one compartment to the other, allowing the flux of solution only through external manifolds. Therefore in this case, the system does not contain central compartments, but just the electrode ones. Result of this experimental measurement is also reported in Fig. 9 for comparison.

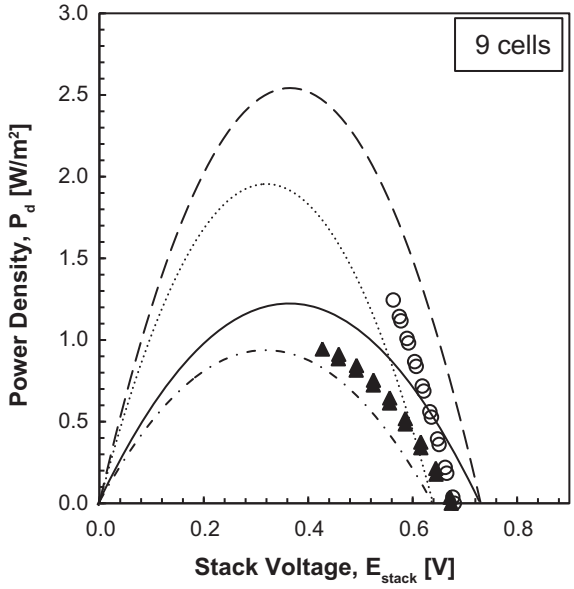

Fig. 13. Model validation for cells stack equipped with 365 μm spacers.
▲Experimental data; ○ "Corrected" data; Model predictions for 9 cells stack: –·–·– $\beta = 0.7$; ____ $\beta = 0.8$; Model predictions for 200 cells stack: ..... $\beta = 0.7$; _ _ _ $\beta = 0.8$.

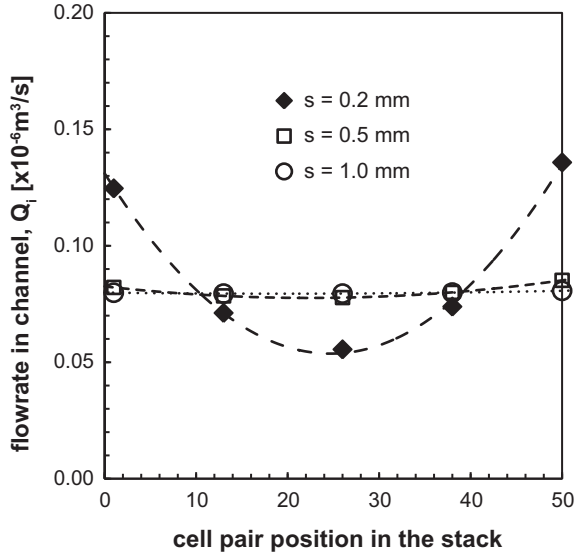

Fig. 14. Estimated flowrates distribution for a 50-cells stack.
CFD simulation of a 50-cells stack with SISO configuration at different distributor thickness. Total feed flow rate: $Q_{tot} = 4 \times 10^{-6}\ m^3/s$; spacer thickness of seawater/brine compartments: $\delta = 200$ μm [17].

Fig. 9 shows a clearly linear dependence of stack resistance on cells number, thus confirming theoretical expectations. On the other side, blank resistance evaluated as intercept of the regression line with the *y*-axis results roughly 10% higher than the experimental value directly measured. Such discrepancy can be attributed to the different configuration of the stack in the blank measurement: in fact, when the stack is equipped with a generic number of cells, the passage of solution between electrode/central compartments cannot be completely avoided; while, in the case of blank measurement, the stack has only a single CEM bathed to both electrode compartments and such effect is absent. Because of this low discrepancy, the extrapolated value from regression line was chosen as measure of R_{blank} for subsequent calculations and model validation.

3.2.2. Electric power and power density

The power output and efficiency for an "ideal" single cell pair, i.e. not affected by the resistance of electrode compartments, has been evaluated by a "corrected" stack voltage, calculated as the product of the overall cells resistance and the current. The cells resistance was calculated from the stack resistance (Fig. 9) subtracting the contribution of the blank. In this way, it is possible to calculate an electric power output, which is not affected by the resistance of the electrode compartments, thus more consistent with the definition given in Eq. (21). Relevant results for 4–6–9–12 cells stack are shown in Figs. 10 and 11. It is worth mentioning that experimental range of current density was rather limited, thus allowing the construction of a small portion of the quadratic trend reported in the figure. On the other side, given the importance

Table 3
Effect of non-uniform flow rates distribution. Summary of case studies. Spacer thickness of seawater/brine compartments: $\delta = 200$ μm [17]

	$s_1 = 0.2$ mm	$s_2 = 0.5$ mm	$s_3 = 1.0$ mm
$Q_{tot,A} = 4 \times 10^{-6}\ m^3/s$ (240 mL/min)	CASE # A1	CASE # A2	CASE # A3
$Q_{tot,B} = 2 \times 10^{-5}\ m^3/s$ (1,200 mL/min)	CASE # B1	CASE # B2	CASE # B3
$Q_{tot,C} = 4 \times 10^{-5}\ m^3/s$ (2,400 mL/min)	CASE # C1	CASE # C2	CASE # C3

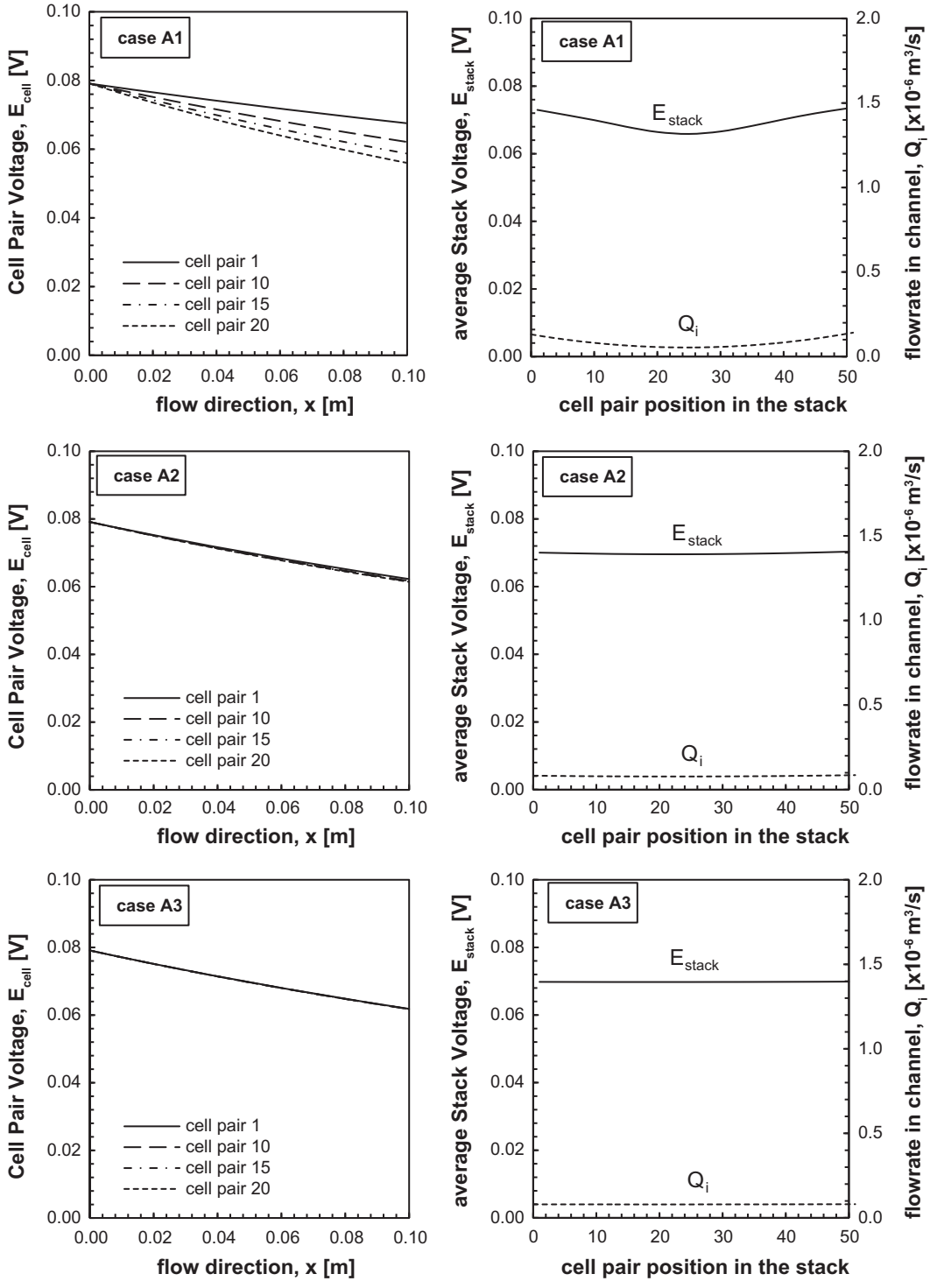

Fig. 15. Effect of non-uniform flowrates distribution on stack voltage (cases A).

of plotting the entire curve in order to evaluate the maximum power output of each configuration, in Section 4 the entire curve predicted by the model is plotted although comparison with experiments is limited to the presented data.

As expected, power output increases when increasing the number of cells (Fig. 10). Moreover, Fig. 11 shows how the "corrected" values of power density are significantly higher than measured values, thus indicating a strong influence of the

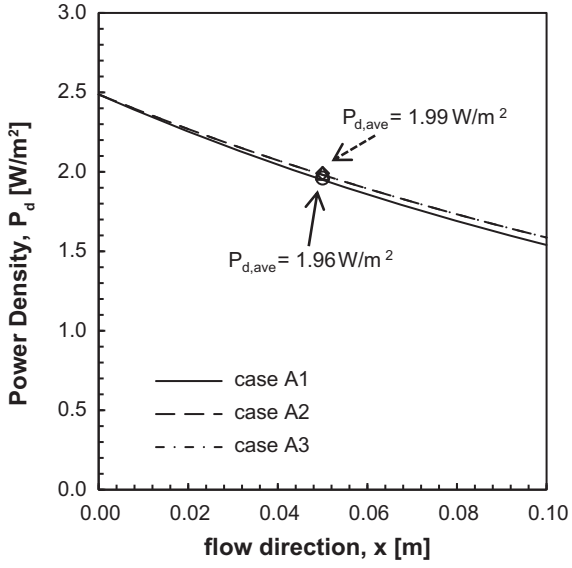

Fig. 16. Effect of non-uniform flowrates distribution on power density (cases A).

blank resistance on the power output especially for stacks with low number of cells.

4. Model results and validation

4.1. Validation procedure and results

A first model tuning/validation has been performed by comparing model predictions and experimental measurements, fixing the operating conditions adopted during experiments and already described in the previous section. In particular, in order to reproduce the tests with variable current density, simulations were performed varying the stack internal current density by acting on the external load (R_u), thus reproducing the same current ramp experimentally imposed by the galvanostat.

Moreover, in order to neglect the effect of blank resistance on total stack resistance and to compare the "corrected power density" values experimentally worked out, simulations of 100, 150 and 200 cell pairs stacks were carried out, finding that already with 200 cell pairs bank resistance was negligible.

A tuning of the adjustable parameter β was also performed, and simulations with values of $\beta = 0.7$ and $\beta = 0.8$ will be shown in the figures.

Model validation results are shown in Fig. 12 for cells stacks equipped with FUJIFILM membranes (specs given in Table 2) and 450 μm woven spacers; the four different cases with 4–6–9–12 cells within the stack have been considered, where flow rates are uniformly distributed in each cell.

Model predictions follow fairly well experimental trends, also indicating the parabolic shape of the power output vs. stack voltage theoretically foreseen.

As physically expected, estimated stack voltage is higher when permselectivity correction factor is increased. However, for the investigated cases, the value of β between 0.70 and 0.80 seems to be able to predict fairly well the system behaviour, with the exception of the case of 12 cell pairs, in which the optimum value for the model parameter seems to be closer to 0.7. However, this discrepancy could be due to non-ideal behaviour of the system, related for example to the presence of non-uniform flow rates distribution and, more importantly, short-cut currents within the stack.

It is worthnoting how such values of β are quite low (the expected reduction of permselectivity passing from 4 to 5 M solution is in the range of 5–10%), thus indicating that such correction factor likely account for other non-ideality factors such as the shadow effect of spacer on membrane, which can undoubtedly reduce the effective membrane area for ion passage.

Validation of the model was carried out also for 365 μm spacers (Fig. 13), and similar considerations apply to this case.

4.2. Effect of non-uniform flow rates distribution: model coupling with CFD simulations [17]

When the assumption of ideal flow rates distribution through the stack is not acceptable anymore, e.g. in the case of a very thin distribution channel, the need for assessing the effect of the real non-uniform distribution arises and requires a more indepth mathematical description of the problem also taking into account the fluid flow behaviour of the system, both in the distribution channels and in each single compartment. This is part of a detailed analysis, which has been performed using computational fluid dynamics (CFD) tools, widely discussed in another work [17].

In this section, the effect of non-uniform flowrates distribution on process efficiency is discussed. Results of CFD simulations of a 50-cells stack with a single-input single-output (SISO) configuration [17] are shown in Fig. 14, showing the flow rates distribution inside the stack using different thicknesses for the distribution channel (s).

CFD results were implemented within the present model by adding an equation relating single channel flow rate to the "normalised number of cell pair",

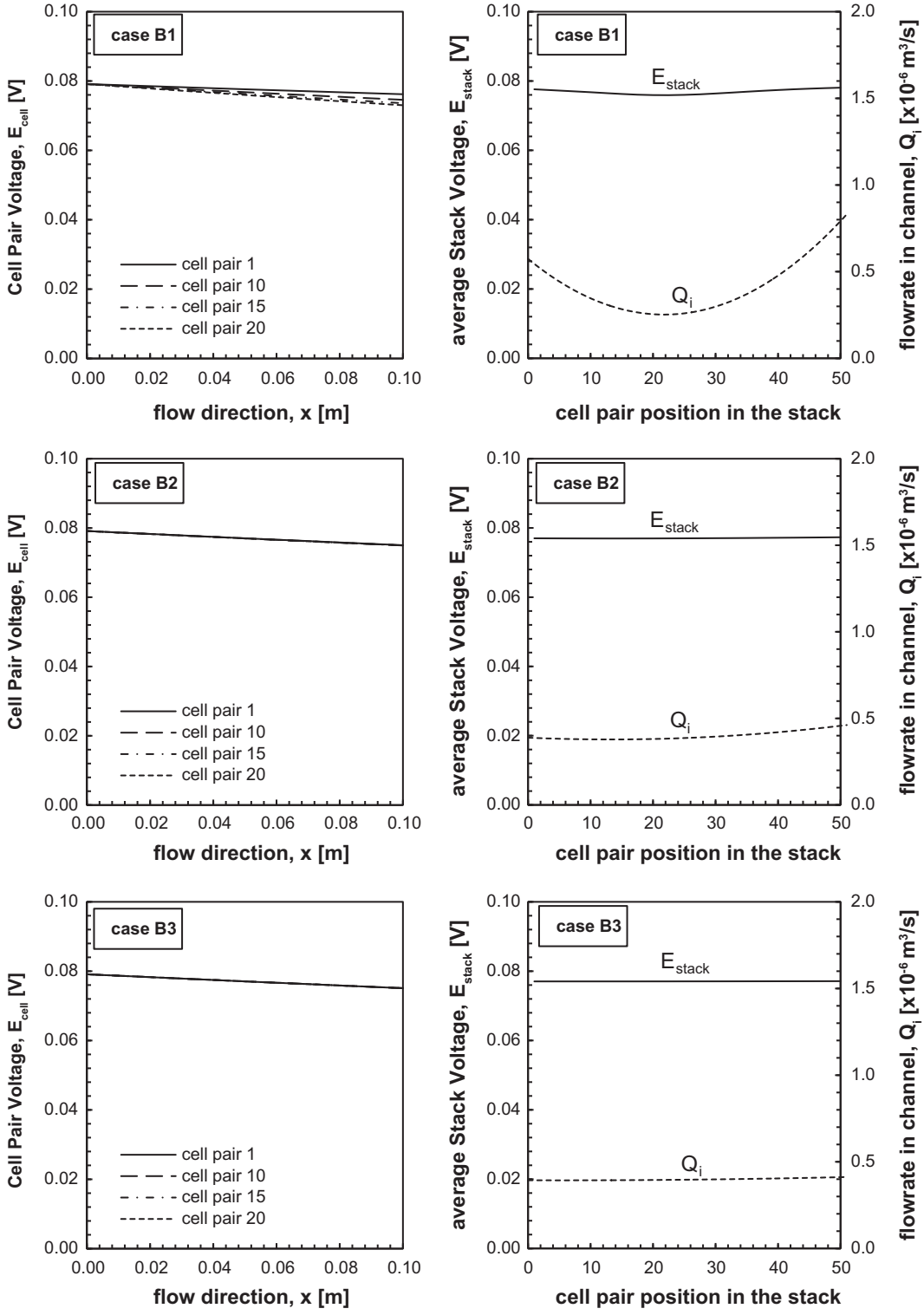

Fig. 17. Effect of non-uniform flowrates distribution on stack voltage (cases B).

defined as the id. number of the cell pair divided by the total number of cells (N). Such equation has been found to have a quadratic form [17] and relevant coefficients were related to the geometrical and operating conditions examined, namely the thickness of distribution channel, s, and total feed flow rate, Q^{tot} (Table 3).

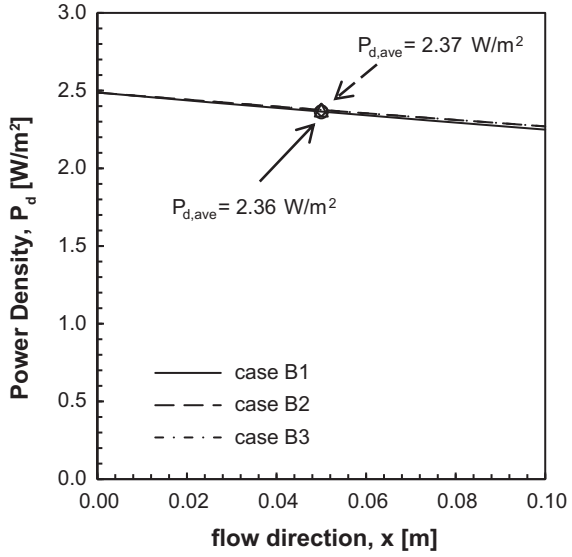

Fig. 18. Effect of non-uniform flowrates distribution on power density (cases B).

Nine case studies were analysed in order to investigate the effect of different flowrates distribution, generated by the three possible values for distributor thickness and total feed flow rate, on process operating and performance parameters (Table 3).

Simulations results related to cases "A" ($Q_{tot,A} = 4 \times 10^{-6}\,m^3/s$) are shown in Fig. 15. Note that in case A1, where the distributor thickness is thinner, the average stack voltage is clearly minimised for the cell pairs in the middle of the stack: this is a consequence of the lower flowrate within these cells, i.e. of the higher residence time within compartments. This effect is rather negligible in the other cases (A2, A3), where a thicker distributor allows more uniform flow rates along the stack [17].

The effect of flow rates distribution on obtainable power density is shown in Fig. 16. Comparing the estimated value of power density for the cases A1–2–3, it can be seen in case A1 (thinner distributor and non-uniform flow rates distribution) a reduction by roughly 5% of the mean power density with respect to cases A2 and A3. At the contrary, for cases A2 and A3 the obtainable power density is nearly the same, due to the very similar flow rates distributions.

A very similar outcome can be observed in Figs. 17–20, were results for cases B and C are shown. Also in this case, the configurations with the thinner distributor channel present a minimum in stack potential for the central cell pairs and, consequently, a reduction in the output power density, which is, however, negligible in all cases. This is likely related also to the very high flow rates in the stack, which keep the driving force in all cell pairs sufficiently high not to affect significantly the overall process performance.

4.2.1. Estimating the obtainable net power

Another important goal achievable through the merging of CFD and process modelling approach has been the estimation of the obtainable electric power from reverse electro-dialysis (RED) system, once the required pumping power has been taking into account. In order to do this, net power is calculated for all of investigated case studies (Table 4), using Eqs. (22) and (23). Results are listed in Table 4. Pressure drop in Table 4 are calculated from CFD simulation and discussed in another work [17] and, although they may refer to an ideal stack geometry, their use can shown of the multiscale approach can be usefully adopted for the simulation of overall process performance.

In particular, Table 4 shows how increasing flow rates generally increases the output power density, but at the same time it can dramatically increase pumping power, thus leading to a negative influence on the net power density. As an example, in case C1, (higher total feed flow rate and thinner distributor thickness), the pressure drop within the system is so high that pumping power is eventually higher than obtainable electric power, thus indicating that an optimal compromise has to be chosen for the overall process optimisation in terms of both geometrical and operating conditions.

4.3. Influence of membrane properties on power density: perspectives for achieving the goal of 8 W/m^2 power generation

A "must" condition for the technological breakthrough of the SGP-RE process is the achievement of a power density sufficiently high to allow for the production of electricity at a cost competitive with other renewable energy technologies. With this regard, one of the main goals of the REAPower project is the development of very thin IEMs in order to reduce dramatically the stack electrical resistance, which is already significantly reduced by the use of highly conductive solutions (seawater instead of river water is used as dilute solution). Increasing and keeping high values of permselectivity for thin membranes is also another important goal, which would allow a remarkable enhancement of the SGP-RE process performance.

On this basis, the model has been adopted for predicting the achievable power density assuming a decrease in membrane thickness (and, proportion-

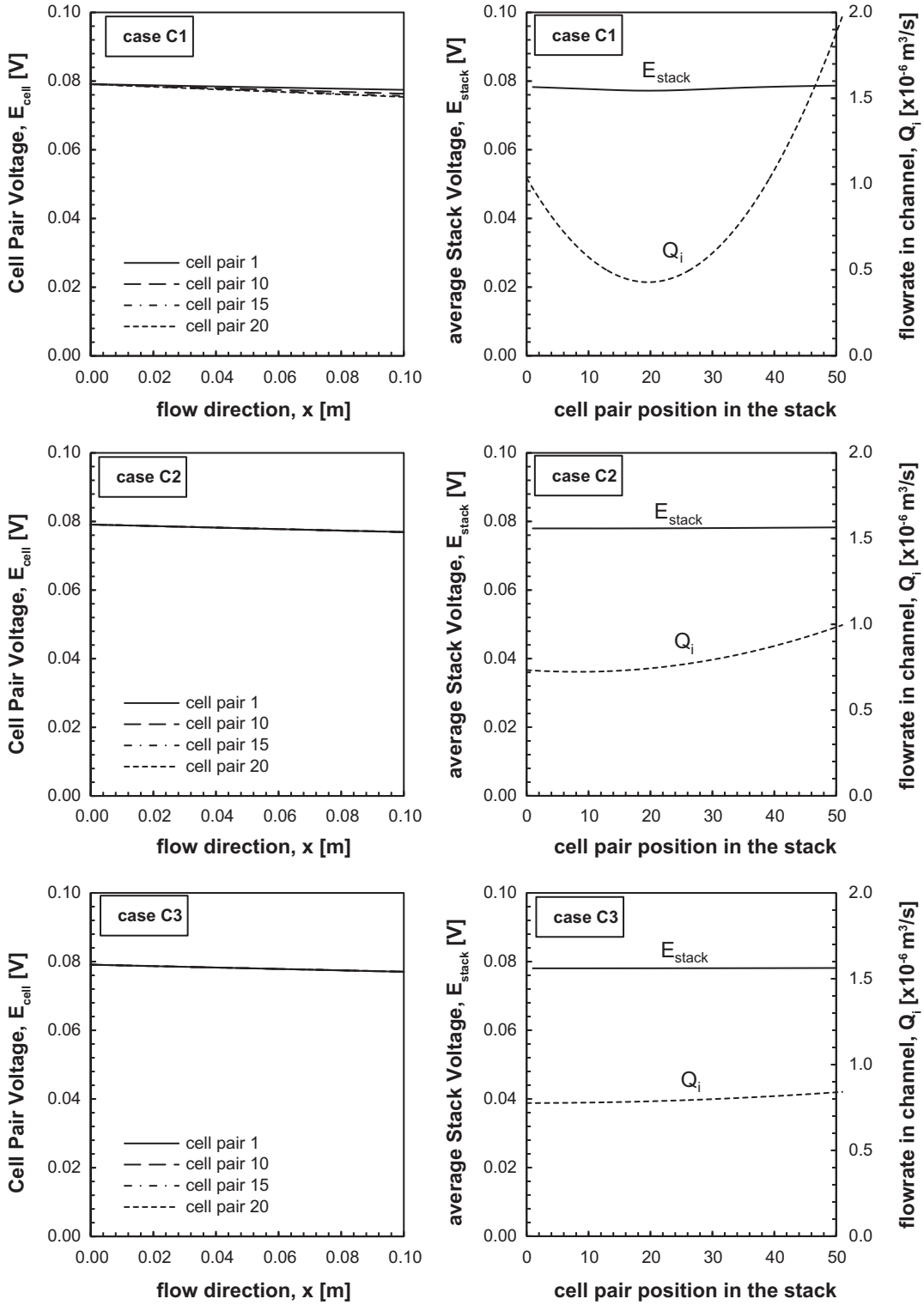

Fig. 19. Effect of non-uniform flowrates distribution on stack voltage (cases C).

ally, also of the IEMs resistance) from the previous 120 μm to values of 20 μm and fixing the AEM permselectivity to the values of 0.65 (as in the standard case shown in previous simulations) and 0.85, which is the target value expected to be reached within the project. The same geometry

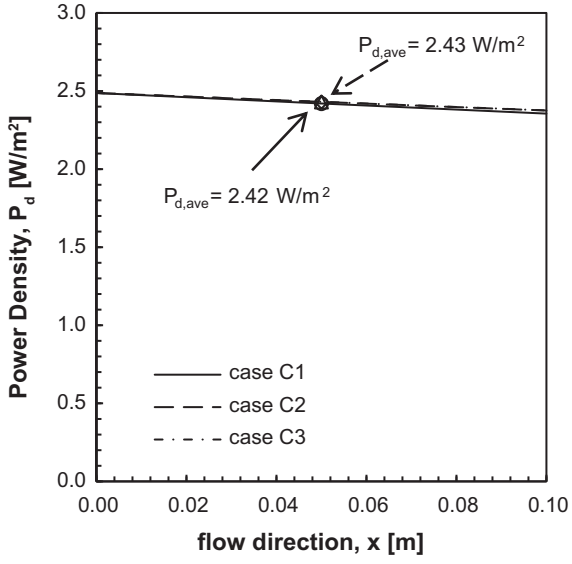

Fig. 20. Effect of non-uniform flowrates distribution on power density (cases C).

adopted in the previous paragraph was used, i.e. spacer thickness of seawater/brine compartments $\delta = 200\,\mu m$ and cell pair dimensions $10 \times 10\,cm$. In order to take into accountof the effect of high salinity and spacer shadow on membrane surface, β value is kept at 0.75, as already done during the model tuning/validation procedure, thus guaranteeing a conservative estimation of predicted values.

A first important remark on the effect of membrane thickness on the stack resistance is IEMs resistance that represents a significant portion of the overall resistance when membrane thickness is around 100 μm, while for thinner membranes seawater compartment resistance may play a dominant role in controlling the overall cell pair resistance. In this respect, a crucial aspect will be the choice of compartment thicknesses. In fact, a thicker brine compartment would allow minor problems of fouling and plugging without significantly affecting the stack resistance, on the other side, seawater compartment will need a thinner spacer, thus requiring a better control of fouling and plugging by a suitable pretreatment of feed solution (see Fig. 21).

Finally, power density predictions are shown in Fig. 22, which indicates how reducing IEMs thickness can significantly enhance the power density, up to values of about $6.7\,W/m^2$ for the 20 μm IEMs and 0.65 AEM permselectivity. Moreover, increasing the AEM permselectivity to the target value of 0.85 would allow for a further raise in power density with a maximum expected value of more than $8.5\,W/m^2$, thus indicating a tremendous potential for improvement of the presented technology.

5. Conclusions

SGP-RE has been recently recognised as a promising technology for energy generation from salinity gradients. Latest interests have also arisen with regard to the exploitation of salinity gradients from brines and seawater, which can guarantee much higher driving forces to the SGP process.

Aim of the present work, carried out within the EU-FP7-funded REAPower project, has been the development of a mathematical model for the SGP-RE process using seawater and concentrated brine.

Starting from a literature review, the model was developed focusing on its capability to simulate the

Table 4
Estimated net power for case studies of Table 3

CASE #	Distributor thickness s (mm)	Feed flow rate Q_{tot} ($\times 10^{-6}\,m^3/s$)	Pressure drop ΔP (Pa)	Pumping power P_{pump} (W)	Power density P_d (W/m^2)	Power output P_{out} (W)	Net power P_{net} (W)	Power losses P_{loss} (%)
A1	0.2	4	1,326	0.015	1.96	0.98	0.97	1.5
A2	0.5	4	391	0.004	1.99	1.00	0.99	0.4
A3	1.0	4	330	0.004	1.99	1.00	0.99	0.4
B1	0.2	20	7,118	0.407	2.36	1.18	0.77	34.4
B2	0.5	20	2,054	0.117	2.37	1.19	1.07	9.9
B3	1.0	20	1,706	0.097	2.37	1.19	1.09	8.2
C1	0.2	40	15,736	1.798	2.42	1.21	−0.59	148.7
C2	0.5	40	4,410	0.504	2.43	1.21	0.71	41.5
C3	1.0	40	3,567	0.408	2.43	1.22	0.81	33.5

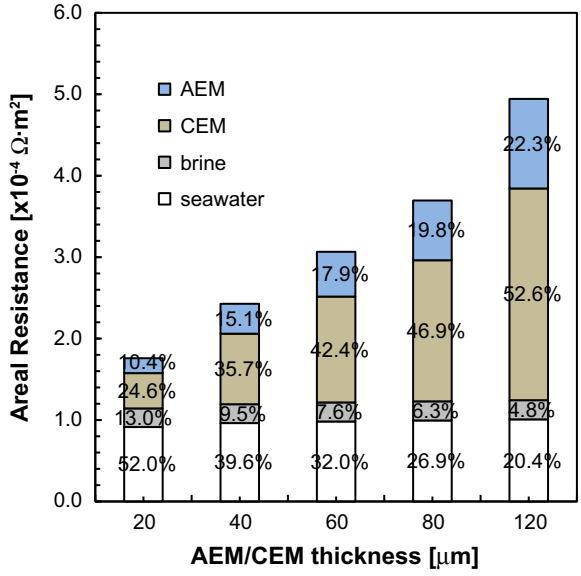

Fig. 21. Influence of IEMs thickness on resistance of the system. Simulation of a 1,000 cells stack assuming a linear decreasing in IEMs resistance with IEMs thickness. $\alpha_{AEM} = 0.65$, $\alpha_{CEM} = 0.90$. Spacer thickness of seawater/brine compartments $\delta = 200\,\mu m$.

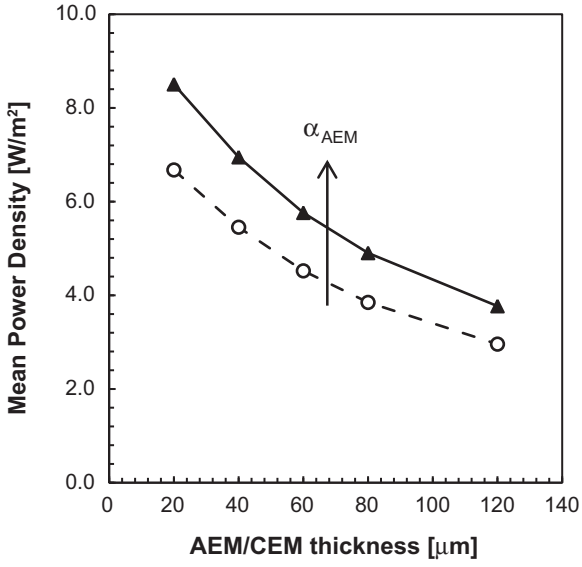

Fig. 22. Effect of IEMs thickness on power density. Simulation of a 1,000 cells stack assuming a linear decreasing in IEMs resistance with IEMs thickness. ▲: $\alpha_{AEM} = 0.65$, $\alpha_{CEM} = 0.90$; ○: $\alpha_{AEM} = 0.85$, $\alpha_{CEM} = 0.90$.

system behaviour when concentrated salt solutions were adopted. A multiscale approach has been used, leading to a multihierarchical model able to predict the effects of operating conditions and geometrical features on the process performance, even allowing the simulation of non-uniform flow rates distribution within a 50-cells stack to the coupling with CFD simulations. The developed model was tuned and validated by comparison with experimental information purposely collected on a laboratory test rig.

Finally, some technology perspectives were also given by performing simulations aiming at the prediction of power density achievable when using thin and selective ionic exchange membranes, indicating the feasibility of reaching a target power density of more than $8.5\,W/m^2$ of cell pair.

Nomenclature

A	—	membrane area (m^2)
b	—	membrane width (m)
B'	—	parameter of Islam et al.' equation ($m^{1/2}\,mol^{-1/2}$)
B'_1	—	parameter of Islam et al.' equation ($S\,m^3\,mol^{-3/2}$)
B'_2	—	parameter of Islam et al.' equation ($m^{3/2}\,mol^{-1/2}$)
B^{γ}	—	second virial coefficient of Pitzer equation ($kg\,mol^{-1}$)
c	—	salt concentration ($mol\,m^{-3}$)
C^{γ}	—	third virial coefficient of Pitzer equation ($Kg^2\,mol^{-2}$)
D_{NaCl}	—	co-ion diffusion coefficient ($m^2\,s^{-1}$)
D_w	—	water diffusion coefficient ($m^2\,s^{-1}$)
E_{stack}	—	stack voltage (V)
F	—	Faraday constant ($96{,}490\,C\,mol^{-1}$)
f	—	obstruction factor (–)
F'	—	parameters of Islam et al.' equation (–)
f^{γ}	—	first virial coefficient of Pitzer equation (–)
I	—	electric current (A)
j	—	current density ($A\,m^{-2}$)
J'_w	—	volumetric water flux ($m^3\,m^{-2}\,s^{-1}$)
J_{coul}, J_{cit}	—	counter-ions/co-ions molar flux ($mol\,m^{-2}\,s^{-1}$)
J_{tot}	—	salt molar flux ($mol\,m^{-2}\,s^{-1}$)
J_w	—	water flux ($mol\,m^{-2}\,s^{-1}$)
L	—	channel length (m)
m	—	electrolyte molal concentration ($mol\,kg^{-1}$)
M_{H_2O}	—	molar weight of water ($18 \times 10^{-3}\,kg\,mol^{-1}$)
N	—	number or cell pairs (–)
P_d	—	power density ($W\,m^{-2}$)
P_{loss}	—	power loss (%)
P_{net}	—	net power output (W)

P_{out} — power output (W)
P_{pump} — pumping power (W)
Q_b, Q_s — brine/seawater flow rate in single channel ($m^3 s^{-1}$)
Q_{tot} — total feed flow rate ($m^3 s^{-1}$)
R — universal gas constant ($8.314 J mol^{-1} K^{-1}$)
R_{AEM}, R_{CEM} — AEM/CEM areal resistance (Ωm^2)
R_b, R_s — brine/seawater areal resistance (Ωm^2)
R_{blank} — electrode compartments (blank) resistance (Ωm^2)
R_{cell} — cell pair resistance (Ωm^2)
R_{stack} — cells stack resistance (Ωm^2)
R_u — external load (Ωm^2)
T — temperature (K)
T_a, T_c — transport number of cation and anion in solution (–)
T_c^{CEM} — transport number of cation into CEM (–)
x — flow direction (m)
z — ion valence (–)

Greek letters

α_{AEM}, α_{CEM} — AEM/CEM permselectivity (–)
β — permselectivity correction factor (–)
$\gamma_{\pm}$ — mean activity coefficient (–)
δ_b, δ_s — brine/seawater compartment thickness (m)
δ_m — membrane thickness (m)
ΔP — pressure drop (Pa)
ε — dielectric constant (–)
η — viscosity of solution (Pa s)
η_P — pump efficiency (–)
Λ — equivalent conductivity ($S m^2 mol^{-1}$)
Λ^0 — equivalent conductivity at infinite dilution ($126.5 \times 10^{-4} S m^2 mol^{-1}$)
ρ_{H_2O} — water density ($1{,}000 kg m^{-3}$)

Acknowledgements

This work has been performed within the REAPower (Reverse Electro dialysis Alternative Power production) project [2], funded by the EU-FP7 programme (Project No. 256736). The authors are very grateful to Winod Bhikhi and Jacko Hessing of FUJIFILM Tilburg Research Laboratories TRL for their support within experimental activities.

References

[1] R.E. Pattle, Production of electric power by mixing fresh and salt water in the hydroelectric pile, Nature 174 (1954) 660.
[2] REAPower, http://reapower.eu/.
[3] H. Strathmann, Ion-Exchange Membrane Separation Processes, Membrane Science and Technology, vol. 9, Elsevier, Amsterdam, 2004, pp. 1–348.
[4] J.N. Weinstein, F.B. Leitz, Electric power from differences in salinity: The dialytic battery, Science 191 (1976) 557–559.
[5] C. Forgacs, R.N. O'Brien, Utilization of membrane processes in the development of non-conventional renewable energy sources, Chem. Can. 31 (1979) 19–21.
[6] R.E. Lacey, Energy by reverse electrodialysis, Ocean Eng. 7 (1980) 1–47.
[7] E. Brauns, Salinity gradient power by reverse electrodialysis: effect of model parameters on electrical power output, Desalination 237 (2009) 379–391.
[8] J. Veerman, J.W. Post, M. Saakes, S.J. Metz, G.J. Harmsen, Reverse electrodialysis: A validated process model for design and optimization, Chem. Eng. J. 166 (2011) 256–268.
[9] J.O.M. Bockris, A.K.N. Reddy, Modern Electrochemistry, vol. 1 (Ionics), Plenum Press, New York, NY, 1998.
[10] K.S. Pitzer, Thermodynamics of electrolytes. I. theoretical basis and general equations, J. Phys. Chem. 77 (1973) 268–277.
[11] National Physical Laboratory UK, http://www.kayelaby.npl.co.uk/chemistry/3_9/3_9_6.html (accessed January, 2012).
[12] S.S. Islam, R.L. Gupta, K. Ismail, Extension of the falkenhagen-leistkelbg to the electrical conductance of concentrated aqueous electrolytes, J. Chem. Eng. Data 36 (1991) 102–104.
[13] A. de Diego, A. Usobiaga, J.M. Madariaga, Critical comparison among equations derived from the falkenhagen model to fit conconductimetric data of concentrated electrolyte solutions, J. Electroanal. Chem. 446 (1998) 177–187.
[14] M. Turek, B. Bandura, Renewable energy by reverse electrodialysis, Desalination 205 (2007) 67–74.
[15] gPROMS Model Builder 3.3.1 (2010).
[16] J. Veerman, R.M. de Jong, M. Saakes, S.J. Metz, G.J. Harmsen, Reverse electrodialysis: Comparison of six commercial membrane pairs on the thermodynamic efficiency and power density., J. Membr. Sci. 343 (2009) 7–15.
[17] L. Gurreri, A. Tamburin, A. Cipollina, G. Micale, CFD analysis of the fluid flow behavior in a reverse electrodialysis stack, Desalination and Water Treatment, 2012, in press. doi: 10.1080/19443994.2012.705966.